Composites Science and Technology 107 (2015) 89–97

Contents lists available at ScienceDirect

Composites Science and Technology

journal homepage: www.elsevier.com/locate/compscitech

Unsupervised learning for classification of acoustic emission events from tensile and bending experiments with open-hole carbon fiber composite samples

Hisham A. Sawan [a], Mark E. Walter [a,*], Brooks Marquette [b]

[a] Department of Mechanical and Aerospace Engineering, The Ohio State University, 201 West 19th Avenue, Scott Laboratory, OH 43210, USA
[b] Honda R&D Americas Inc, 21001 State Route 739, Raymond, OH 43067, USA

ARTICLE INFO

Article history:
Received 28 May 2014
Received in revised form 25 November 2014
Accepted 4 December 2014
Available online 11 December 2014

Keywords:
D. Acoustic emission
A. Carbon fibres
Unsupervised learning

ABSTRACT

Widespread use of composites for structural applications is hindered by the inability to fully understand and predict the materials response. The uncertainty in composite materials response is largely due to variability in the initiation and propagation of damage. To develop new tools for design with composite materials, techniques for identifying damage modes during operation are needed. While there is a large body of work on analysis of acoustic emission (AE) from different materials and different loading cases, the current research is focused on applying unsupervised learning for separating AE into a maximum number of groups with distinct evolution. AE data was collected during tensile and bending experiments on carbon fiber reinforced epoxy specimens with different material configurations. The unsupervised learning algorithms successfully identified AE groups with distinct initiation and evolution. With damage mechanisms inferred from load response and from deformation fields obtained with digital image correlation (DIC), strong correlations between the behaviors of the groups and the damage mechanisms were observed and are discussed.

1. Introduction

Composite materials are used extensively in the aerospace industry for their high strength and stiffness to weight ratios and the ability to tailor materials for desired properties. Only relatively recently has the automotive industry become more interested in composite materials for improved fuel economy by light-weighting and improved crash performance by energy absorption. However, unlike metals, fiber-reinforced composites experience many damage types, such as matrix cracking, fiber/matrix pull-out, fiber breakage, and delamination. A major challenge to wide-spread implementation of composites is this wide variety of damage mechanisms associated with composite materials and understanding how those mechanisms initiate and progress. The complicated failure processes in composites precludes the use of current design methodologies.

To develop new and necessary tools for designing with composite materials, it is critical to quantify the damage state at different load levels. Knowing the damage state would allow for an iterative design process and ultimately lead to high fidelity predictive tools. Several methods have been investigated to measure the damage state. For carbon fiber reinforced polymers (CFRPs), these methods can be broadly grouped into the following categories: bulk electrical property sensing, embedded sensing, and surface-based sensing. Electrical methods utilize the fact that initiation and progression of damage cause changes in conduction paths which in turn affects bulk electrical resistance and capacitance [1,2,3]. The most common embedded sensing method is with fiber Bragg gratings (FBGs) which monitor changes in internal strain [4]. In addition, FBGs can sense vibration resulting from damage events [5]. Surface sensing techniques typically require interpretation of either surface deformation or vibration. Surface deformation can indicate localized stiffness reduction and, hence, damage [6]. Surface vibrations can be measured in the form of acoustic emission (AE), which are stress waves resulting from rapid release of strain energy. These waves can be sensed at specimen surfaces with piezoelectric sensors and relevant data acquisition and interpretation apparatus [7].

AE from material damage in composites is relatively easy to monitor and record. However, efficient and effective analysis is still challenging. Efforts have been made to predict failure load based on AE. For example, to predict the final failure load based on AE from loading a sample to about half its expected failure load,

* Corresponding author. Tel.: +1 614 292 6081; fax: +1 614 292 3163.
E-mail address: walter.80@osu.edu (M.E. Walter).

http://dx.doi.org/10.1016/j.compscitech.2014.12.003
0266-3538/

Sasikumar did supervised learning with an artificial neural network [8]. Others used AE to estimate the location of damage in relatively large structures. Locating damage can be challenging due to the existence of multiple wave modes which propagate with different velocities [9]. The directional effects on the properties of acoustic waves travelling in anisotropic materials also adds to the location estimation challenges.

A different class of AE analyses aims to find the acoustic signature of damage mechanisms. This type of AE analysis involves separating AE signals into groups that represent different damage mechanisms. This process is called clustering. Clustering involves three components. The first is choosing the signal features to base clustering on. The second is identifying the right number of clusters. The third is the technique with which clustering is achieved. These three topics are discussed next.

Different aspects of the AE signals can be used for clustering. Clustering can be based on temporal AE signals. As shown in Fig. 1, relevant temporal features include signal amplitude, duration, energy, and rise time. But AE signals generated by damage (microcracks, debonding, etc.) are generally not stationary [10]. Therefore, clustering is also often based on other signal features, which are extracted from the signal's frequency domain [10]. Such features include the frequency at maximum amplitude and the frequency at center of area under frequency response curve. Frequency domain features are obtained from fast Fourier transform or a more general wavelet transform. Wavelet analysis involves breaking down the signal into a series of orthogonal basis functions of finite length called wavelets instead of breaking it down into harmonic functions [11]. Extra indices can be calculated from combinations of the previous temporal and frequency domain features. These extra indices include average frequency and slope, which is the ratio of amplitude to rise time. Besides focusing on pure AE features, functions combining AE signal features and mechanical information have been used to understand damage progression. For instance, Bakhtiary used the logarithm of the ratio between strain energy and acoustic energy to identify the onset of delamination and its progression in glass fiber/epoxy composite material [12].

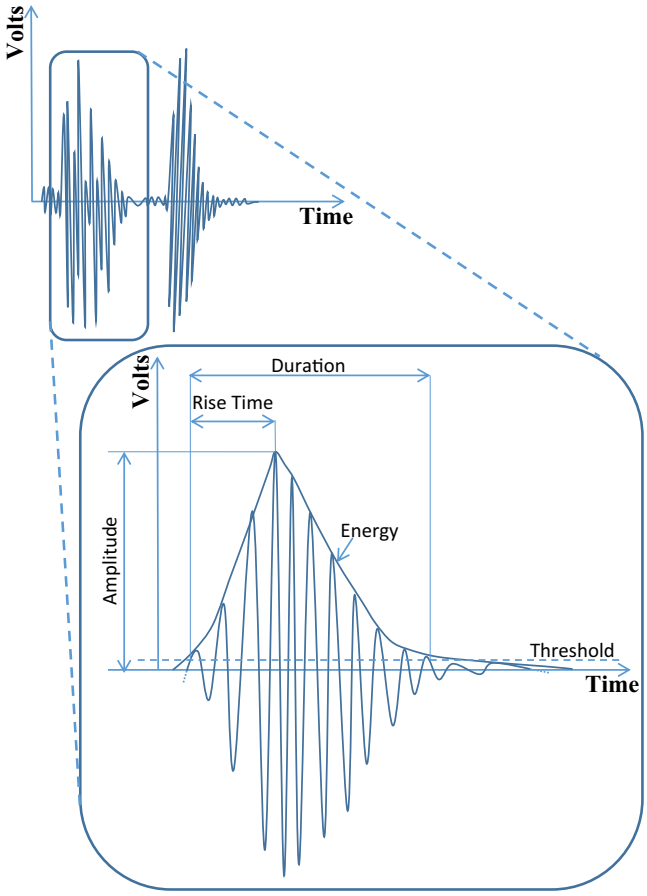

Fig. 1. A schematic AE signal with several AE signal features identified.

Clustering generally requires specifying a desired number of clusters. There exist many cluster validity techniques for determining an optimal number of clusters. These techniques are numerical measures of how unique the resulting clusters are. These numerical techniques include the Silhouette method, Dunn's (DN) index, Davies–Bouldin (DB) index, Krzanowski–Lai index, Hartigan index, and the Calinski–Harabasz index [13]. The DB index is proportional to the ratio of scatter within clusters to their separation. The DN index is the ratio of the minimum distance between two events of different clusters to the maximum distance between events of the same clusters [14]. Each index should have a certain behavior at the optimum number of clusters. For instance, a minimum DB index, a maximum DN index, or a sudden change in either of the two is expected to indicate the optimum number of clusters [14]. The numerical techniques, however, sometimes fail to predict the right optimum number of clusters. For instance, Maulik and Bandyopadhyay showed that even for well-separated clusters, a more complicated index was needed for successful prediction [14].

The clustering process can be achieved through automated data mining which recognizes patterns in complex data sets [15]. This data mining process will henceforth be called unsupervised learning. Unsupervised learning has a wide range of applications including marketing problems [16], motion analysis [17], and speech recognition [18]. Several unsupervised learning techniques exist. One famous technique is the k-means method which formulates the clustering problem as an optimization problem to which a numerical solution can be reached through an iterative process [19]. Another technique is the self-organizing map, which is an application of an artificial neural network that maps the data space onto a two dimensional space where similar data items are located close to each other on the map [13]. Other techniques assume the data follows a distribution density function. Although following a density function is not typically assumed for finding the AE signature of damage, Farhidzadeh et al. developed a criterion for crack classification by assuming that AE data followed a Gaussian distribution [20].

In this paper, numerical clustering-quality indicators are not used for finding the optimum number of clusters which is enforced during clustering. Instead, the maximum number of distinct AE groups is sought. Distinct groups are those that show distinct evolution throughout loading and have statistically representable numbers of observations. Gaussian distribution is assumed for clustering as it was tested on artificial data and found to have better performance than other techniques. This paper is organized into three main sections. The experimental section provides details about the samples and testing equipment used to acquire features of AE signals as well as the deformation and kinetic responses that will represent damage. The section on unsupervised learning explores and compares different methods for choosing the number of clusters and unsupervised learning technique. Then, a separate section presents and discusses the results of clustering performed on AE collected from experiments with CFRP composites. Several distinct groups were separated and correlated to damage mechanisms as inferred from load response and from deformation fields obtained with digital image correlation.

2. Experimental

The CFRP samples had fibers from Panex 35 from Zoltek and SC-15 epoxy from Applied Poleramic. The University of Dayton Research Institute manufactured the samples using a wet layup process. The thickness per ply was about 0.26 mm. All the samples were 36-mm wide, 250-mm long, and with a 6-mm diameter hole in the center. Several configurations were manufactured and tested. The following layups were studied: $[\pm 45^\circ]_{5s}$, unidirectional $[0^\circ]_6$, and $[0^\circ/90^\circ/-45^\circ/+45^\circ/0^\circ/90^\circ/-45^\circ/+45^\circ/0^\circ/90^\circ]_s$ with four added 0° plies. The subscript "*s*" denotes symmetric and the number in subscript denotes the number of repetitions. The four added 0° plies covered the specimen width and approximately 27 mm in the middle of the samples' length. Since the plies were added to the flat tool first, the side with the ply additions was flat.

All testing was conducted at room temperature with displacement control mode at a constant rate of 2 mm/min for tension and 1 mm/min for 4-pt bending. The samples tested in tension had 56-mm long tabs at each end. The 4-pt bending experiments had an outer span of 166 mm, an inner span of 83 mm, and loading pins of 6-mm diameters. The load frame used was a servo-hydraulic MTS model 312.31 with 250-kN capacity. Pneumatic wedge grips, rated for 100 kN, held the samples at the tabs for tension testing. The upper grip was attached to an MTS model 661-23A-01 load cell rated for 250 kN. The lower grip was attached to the moving piston.

Head displacement and load were recorded for all experiments. Deformation fields on the sample surfaces were also measured using 3D digital image correlation (DIC). DIC is a non-contact technique which depends on tracking subsets of light intensities from images of the sample surface before and after deformation [21]. Since two cameras with non-coincident optical axes are used for simultaneous image capture, 3D surface deformation can be determined [22].

A high fidelity, wideband SE 100-H sensor from Vallen Systeme was used to monitor AE. This sensor has a flat response over a frequency range of 8–400 kHz. The couplant used was plasticine, a type of clay that offers high performance comparable to superglue [23] but remains soft and does not cause permanent attachment. The sensor was used with a Vallen AMSY-5 AE acquisition system which includes an AEP4 preamplifier. The Vallen hardware is capable of reducing the AE signals into a set of features such as amplitude, duration, and energy. The Vallen software has the ability to also record the transient signal and post-process it for obtaining the frequency domain signal features. Also, load and head displacement data was fed to the Vallen system and recorded at a 10-Hz sampling frequency. The AE signal features and load data were imported into MATLAB® for subsequent processing and visualization. For most of the plots, the dependent variable was normalized by its maximum value.

3. Unsupervised learning

Several MATLAB functions do clustering of data sets based on indices. A data set may be composed of hundreds of observations. Each observation is described in terms of its own values for the different indices. As discussed earlier, amplitude and frequency are appropriate indices associated with AE observations. The following four MATLAB functions were investigated for application to AE data: k-means, hierarchal, fuzzy c-means, and Gaussian mixture distribution (GMD). K-means and hierarchal clustering aim to divide data points into clear groups based on the indices. The k-means algorithm is an iterative partitioning of data that minimizes the total sum of the within-cluster point-to-cluster centroid distances (MathWorks). On the other hand, the hierarchal clustering algorithm starts with individual observations as separate clusters, and then reduces the number of clusters by finding the two closest clusters and combining them into one. This process is repeated, reducing the number of clusters by one at each time, until the desired number is achieved. The fuzzy c-means function does not seek clear separation of observations, but assigns a membership number to each observation. The membership ranges from 0 to 1. An observation's memberships to all clusters sum to 1. A higher cluster membership value indicates that that observation is more likely to belong to that cluster. GMD assumes the data in each group follows a Gaussian probability density function (PDF). The function that finds the PDF parameters is based on an expectation–maximization (EM) technique. Although EM was used with the assumption of Gaussian distribution in this paper, it can find parameters of a different PDF if needed [24].

To investigate which of the four functions described above works best for AE data sets, an artificial data set with features similar to AE observations was constructed and then analyzed with each of the four functions. The artificial data set had hundreds of observations or events described by two relevant indices and 3 indices of random numbers that simulated irrelevant AE variables. At the same time there were three regions within the data set that had different distribution densities. Fig. 2 shows the results from each clustering attempt. Each color is within a dotted line region and represents data belonging to one cluster. The goal of this analysis was to compare the ability of each of the four functions to distinguish between the regions with different densities, separating the data into the three groups encircled in Fig. 2d.

As seen in Fig. 2, the Gaussian mixture distribution method gives the most desirable results where the two small groups are clearly separated from one another and from the larger group. On the other hand, k-means and hierarchal clustering techniques fail to separate the two small groups from each other, while fuzzy clustering entirely associates one small group with part of the larger group.

There are two reasons why actual AE data needs to be divided into more clusters than expected from the number of active damage mechanisms. First, as observed in Fig. 2d, the artificial data points in the wide range, low density group had to be divided into several overlapping clusters to avoid misrepresentative grouping. As will be shown later, this observation justifies the separation of experimental data into more clusters than expected. The second reason is more relevant to observations from actual experiments than to artificial data. In experiments, one damage mechanism can be responsible for several AE groups of different feature ranges. For example, Prosser et al. reported that, due to attenuation, single mechanism such as a matrix crack can produce signals of various amplitudes [9]. Two AE groups from different damage mechanisms may contain indices more similar to each other than to other groups even from their own damage mechanisms. Assuming this case occurs, enforcing a small number of clusters will cause the two groups from different damage types to be combined. The evolution behavior of the combined cluster can no longer be correlated to a certain mechanism as combining them will suppress trends in the evolution of individual clusters.

Variations in the damage sources associated with the same mechanism most probably exist. These source variations and variations in signal paths may follow certain distribution functions. In that case, the features of emitted acoustic signals will also follow distribution functions with corresponding function densities and ranges. Unlike the other unsupervised learning algorithms, GMD assumes observations of a certain cluster follow a distribution function, namely Gaussian. Furthermore, GMD allows for versatility in parameters of distributions corresponding to the different clusters. As a result, GMD avoids assigning data from low-density groups to other neighboring clusters such as the case shown in Fig. 2c from fuzzy clustering. Since the GMD method is expected

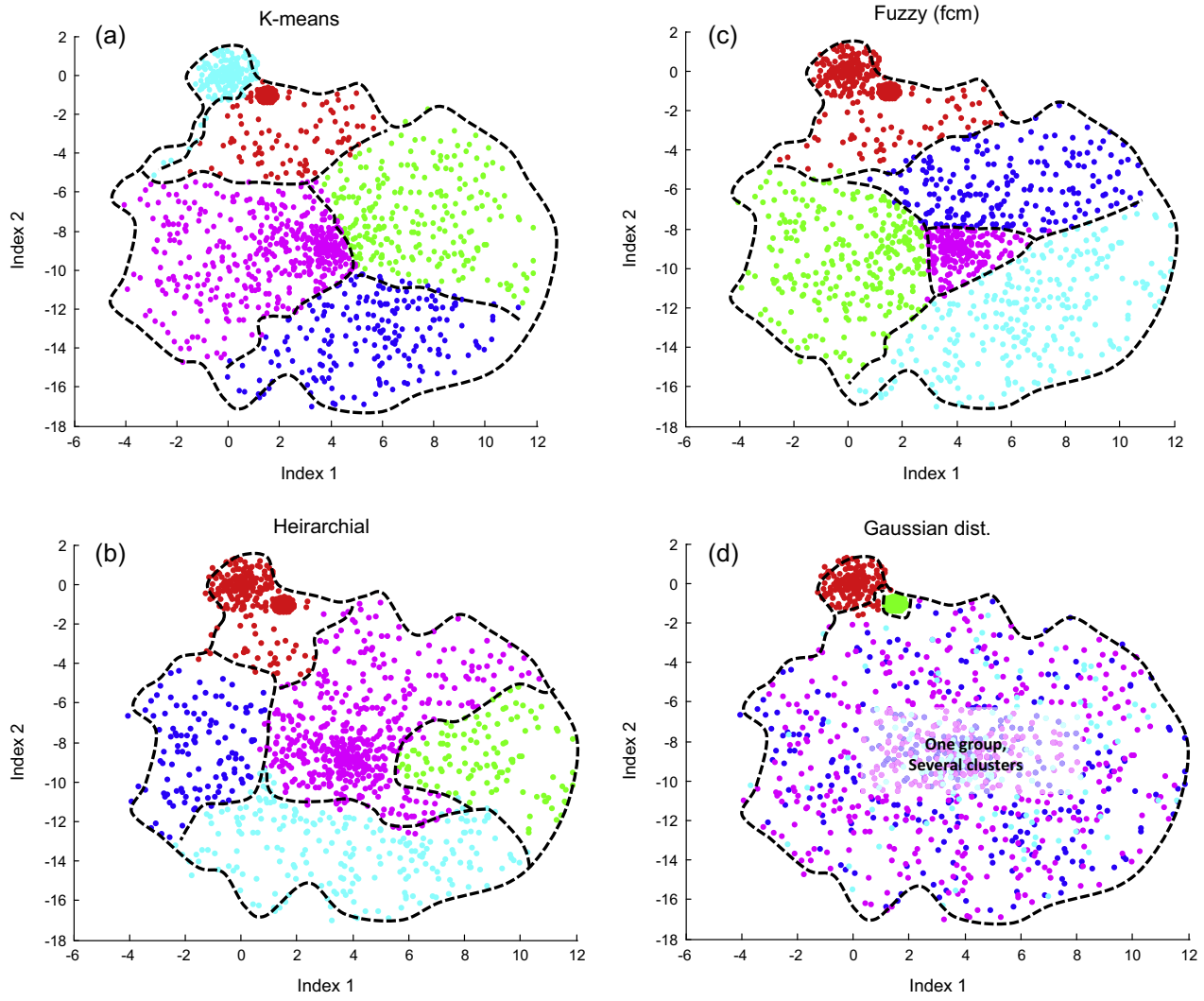

Fig. 2. Applying MATLAB clustering techniques to artificial data: (a) K-means algorithm, (b) hierarchial clustering, (c) fuzzy clustering and (d) GMD achieved with EM algorithm.

to work better with AE data, the rest of the analysis presented in this paper uses GMD.

4. Results and discussion

The AE indices used for clustering included five temporal signal features, two frequency domain features, and two derived indices. All available indices were used for clustering as it was not certain which ones were most relevant. Although having many irrelevant indices is not desirable as it is more time consuming and may hinder converging to a solution; GMD was shown in the previous section to be effective even when there were more irrelevant indices than relevant ones. The temporal features that were used consisted of: amplitude, rise time, energy, counts, and duration. The frequency domain features are the frequency at maximum amplitude and center of area under the frequency response curve. The two derived indices were (a) average frequency and (b) slope, which is ratio of amplitude to rise time.

AE cluster behavior and damage evolution were assessed and compared to each other. Damage was inferred from (a) change in slope of the load-axial strain curve or shear strain-axial curve and/or (b) progression of a damage front as tracked by DIC. Conclusions regarding the behavior of AE clusters were based on event rate and cumulative event count of individual clusters. If one damage type is the exclusive source of an AE cluster, both damage and the accumulation of event clusters would start together. On the other hand, if several damage types contribute to AE activity in one cluster, the activity rate is expected to noticeably change whenever damage of a corresponding type starts. For easier observation of the AE behavior and because AE clusters encompassed different number of events, the cumulative AE is always normalized to the total number of events in the cluster. AE events from different samples were analyzed separately and their results are presented and discussed in separate sections below.

4.1. ±45-degree samples

Clustering was performed on AE data from testing the ±45° samples exposed to tensile loading. The effectiveness of numerical validity techniques for finding the optimum number of clusters was first investigated. As Fig. 3 shows, the DB and DN indicators suggest that either three or five clusters are optimal since a sudden increase in DN and decrease in DB are observed. Moreover, compared to five clusters, since six clusters have a higher DB index and much lower DN index, one would expect six clusters to be far less representative compared to five clusters. However, compared

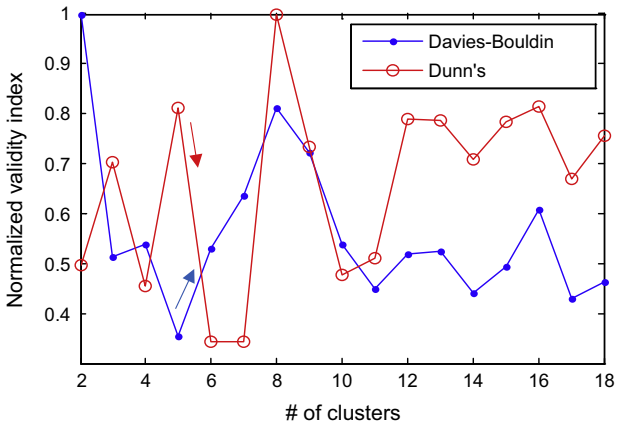

Fig. 3. The DB and DN numerical indicators for predicting optimal numbers of clusters.

to the case of five clusters shown in Fig. 4a, the case of six clusters reveals two additional distinct evolution patterns that are indicated by the arrows in Fig. 4b. Contrary to what the numerical indicators suggest, neither three nor five is the optimum number of clusters since six clusters give the largest number of unique clusters. The numerical techniques, therefore, fail to identify the right number of distinct clusters.

Several clusters in Fig. 4 have similar evolution behaviors and can be combined into a fewer number of clusters with distinct behaviors. For the present work, combining the clusters was done manually after observing similarities in cluster behavior throughout a given test. In Fig. 4b there is a maximum of four distinct, statistically representable AE clusters. Fig. 5 shows these combined clusters which will be henceforth called "groups." No group has less than 580 members, which gives an indication of how statistically acceptable the groups are. In the following sections, only groups are shown and discussed.

As labeled in Fig. 5, the four distinct groups will be referred to as groups A, B, C, and D. As marked by the cross on the normalized load curve in Fig. 5, events in group A start accumulating very early in the test, close to when the slope of load curve starts changing. On the other hand, as marked by the cross on the normalized ε_{xy} curve, events of group B start later, close to when the shear strain deviates from linearity. Group C, unlike the other clusters, is active mainly in a short intermediate section of the test, whereas group D shows significant activity throughout the test. It is a significant fact that the four AE groups have dissimilar activity patterns. This fact indicates that they correspond to different damage phases through the test.

Five samples were tested. The samples failed at a mean load of 21.6 kN with a standard deviation of 440.7 N. AE analysis was performed on data from three samples. The repeatability of the load response and the AE clustering analysis can be seen in Fig. 6.

4.2. Unidirectional 0-degree sample

This section presents results for a sample made from six 0° plies, with a total thickness of 1.56 mm. During loading, a longitudinal crack started tangential to the hole. As seen in Fig. 7, the crack proceeded outwards, towards the grips, until the sample separated at the crack plane. Since damage propagated along the length of the specimen, there is no uniform, far-field region where average strain can be determined. Thus all plots presented in this section use cross-head displacement instead of strain. To correlate the just-described damage with AE activity, a measure of the damage activity was formulated. The damage activity, as presented in Fig. 8, is the product of the length of the intact area and the strain level in the area where the crack eventually occurs. When loading starts, the whole sample is intact, but the strain level is low which gives a low slope of the damage activity measure. Towards the end of the test and although the strain level is high, again the damage activity measure has low slope due to the prevailing effect of a diminishing intact portion.

The AE analysis for this sample gives two groups, or distinct AE clusters, which correlate to damage evolution. As shown and labeled in Fig. 9, events in group A show minimal activity after some point in the test. This observation correlates with the fact

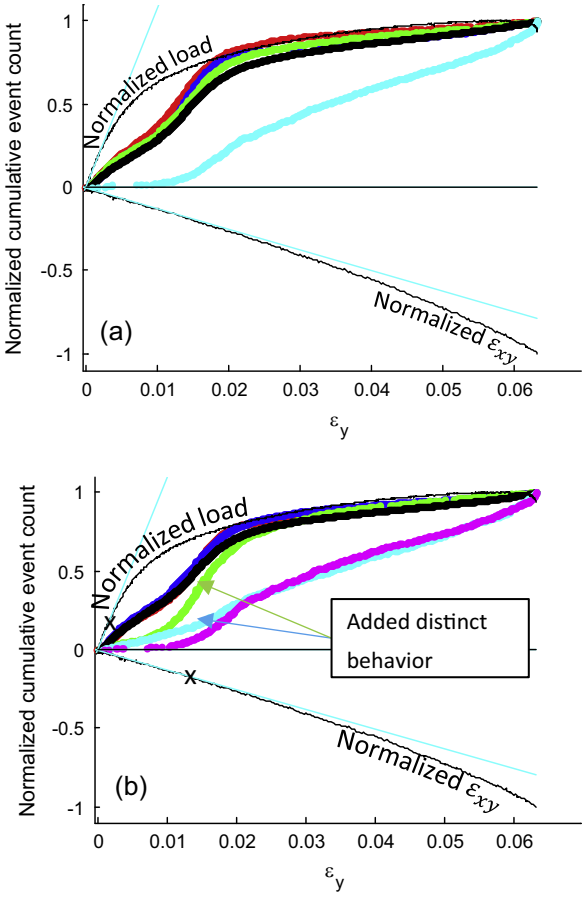

Fig. 4. Behavior of AE in the cases of (a) five clusters and (b) six clusters.

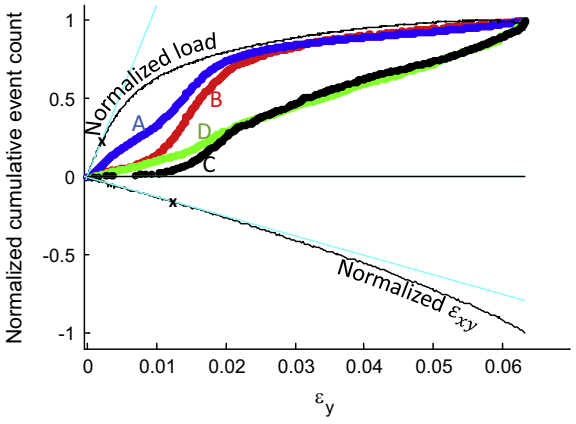

Fig. 5. Grouped AE data after combining the Fig. 5b clusters with similar evolution.

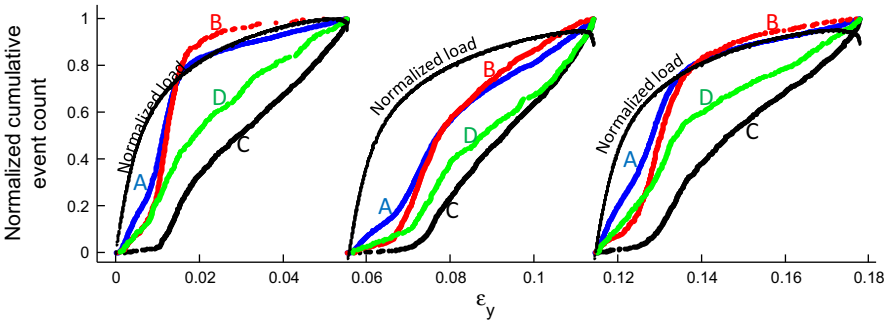

Fig. 6. Comparison of load response and AE analysis results for three identical experiments with 45° samples.

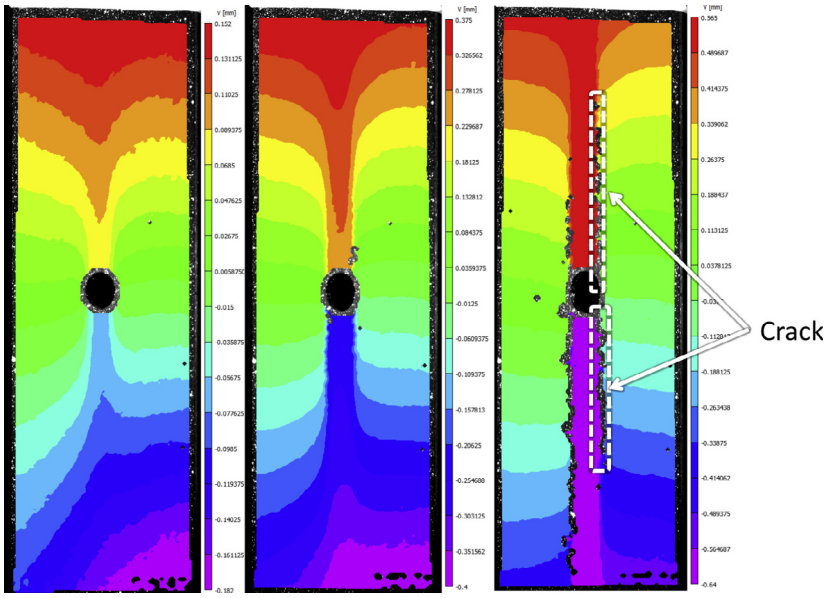

Fig. 7. Axial displacement field of the 0° sample as damage progresses: at 25%, 60%, and 75% of the test.

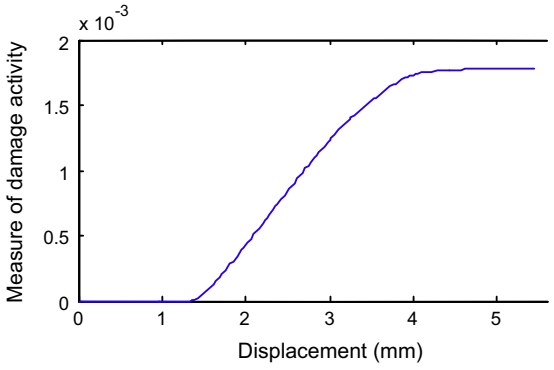

Fig. 8. Evolution of the measure of damage activity for unidirectional 0° samples with a hole.

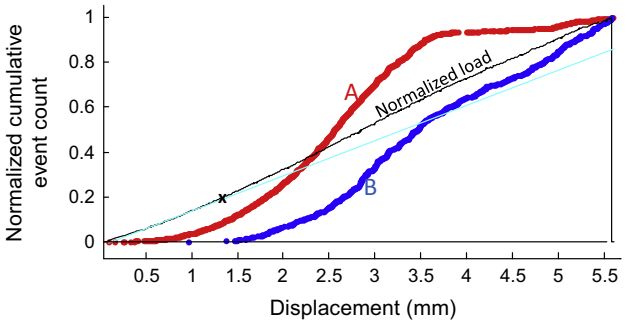

Fig. 9. Behavior of the different AE clusters as well as the load response for unidirectional 0° samples with a hole.

that damage saturation is realized well before final failure as shown in Fig. 8. This correlation suggests that the acoustic signals belonging to group A are emitted by the propagating crack.

Group B behavior correlates to fiber-related damage. The point where load deviates from linearity is marked by a cross on the load curve in Fig. 9 where load slope starts increasing. The stiffening of the sample could entail alignment of curved or initially misaligned fibers. Intact fibers existed until final failure occurred. Events of group B started later, close to when the load curve deviates from linearity; group B remained active until final failure, not showing the saturation seen in group A. Therefore, group B could have been triggered by fiber-related damage which started at the load deviation point and ended with final failure. Furthermore, group B is characterized by higher duration, energy, and amplitude values compared to group A. This observation also suggests group B is triggered by fiber-related damage, which is expected to emit greater strain energy than that related to matrix failure.

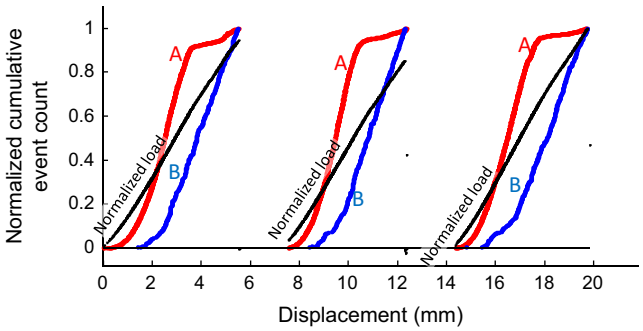

Fig. 10. Comparison of load response and AE analysis results for three identical experiments with 0° samples.

Five samples were tested. The samples failed at a mean load of 58.2 kN with a standard deviation of 7.4 kN. AE analysis was performed on data from three samples. The repeatability of the linear load response and the AE clustering analysis can be seen in Fig. 10.

4.3. Tension sample with added plies

The sample configuration studied in this section is $[0°/90°/-45°/+45°/0°/90°/-45°/+45°/0°/90°]_s$ with four 0° plies added around the hole, on the flat side of the sample. The locally added 0° plies stiffened only one face of the sample, thus adding asymmetry. The sample was also geometrically asymmetric as one side was flat and, due to the local insertion of the four additional plies, the other side was not flat. Under tension the sample experienced out-of-plane displacement, in the thickness direction. Both the geometric asymmetry and asymmetric configuration of ply orientation contributed to this out-of-plane displacement, which was measured by DIC.

The linear elastic portion of the test was expected to have linear relationship between the out-of-plane displacement and axial strain as well as between load and the axial strain. This linearity in out-of-plane displacement can be seen in Fig. 11a. Because a damaged sample is less stiff than an intact sample and would enforce less deflection on the fixed grips at the same load, the point of deviation from linearity potentially indicates the start of damage. It was observed that the additional 0° plies eventually separate at failure. Therefore the damage marked by the displacement drop is most likely shear damage in the interface between the continuous plies and the four added plies.

Clustering of the AE data for this sample gives two AE groups, which correlate to damage evolution. Events in group A started accumulating very early in the test as shown in Fig. 11b. On the other hand, events of group B started later, close to when the out-of-plane displacement curve started deviating from linearity as shown in Fig. 11a. This correlation suggests that the AE events associated with the second group were emitted by the shear damage between the plies. As seen in Fig. 12, group B activity was more intense as the signal amplitude, duration, and energy are significantly higher than those of group A. In terms of repeatability, three samples were tested and the failure load ranged from 58.3 to 64.4 kN. Fig. 13 shows the repeatability of the AE analysis' results and correlation to out-of-plane displacement.

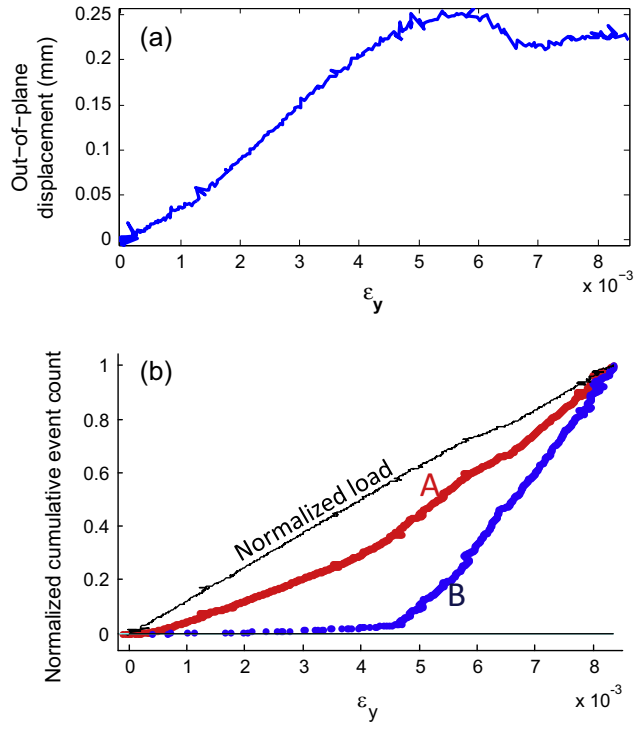

Fig. 11. (a) Out-of-plane displacement. (b) AE behavior as well as load response.

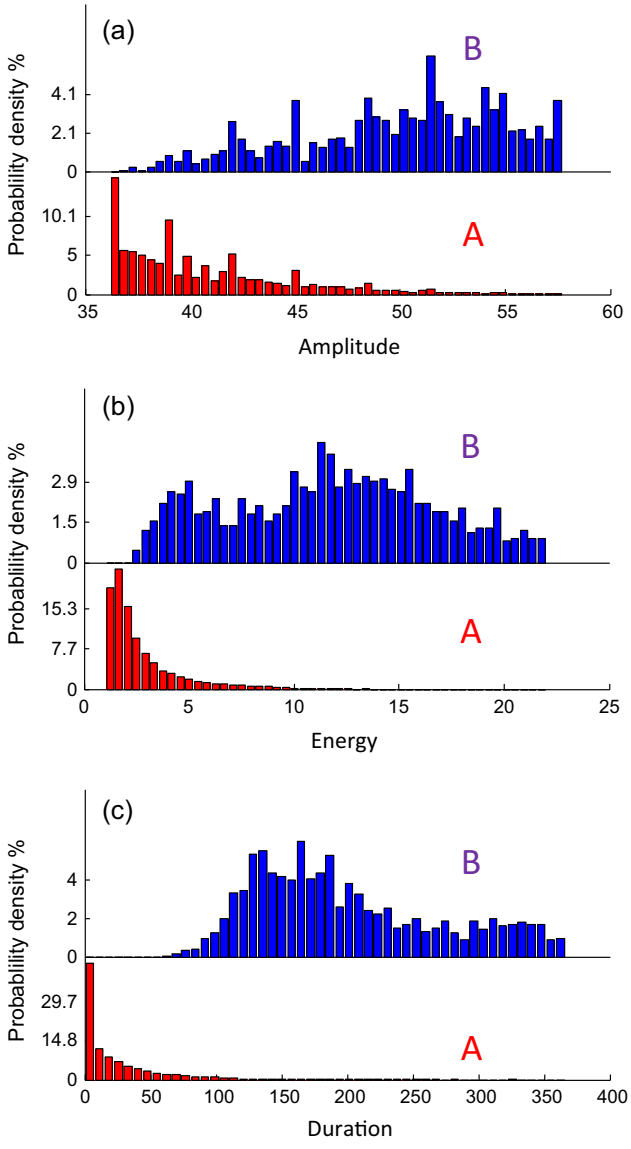

Fig. 12. Event distribution per cluster A and B for the signal: (a) amplitude (dB), (b) energy and (c) duration (μs).

4.4. Bending sample with added plies

Open-hole samples with the same, just described, layup configuration and added plies were tested under 4-point bending. The flat side of the sample, where the added plies are, was on the tension side. Since the four loading points and the center hole did not allow for clear far-field conditions for strain measurement, all plots of this section use cross-head displacement instead of strain. The load curve shows many more drops compared to the case of tensile loading. AE analysis aims to correlate the behavior of different AE groups to the different load drop instances.

As can be seen in Fig. 14, five AE groups can be separated. Group A showed no activity after the largest load drop which is labeled "drop 2" in Fig. 14. Group B showed reduced activity after the same load drop, but remained active. Group E started after the same load drop and remained active until the test ended. Group D started early and its activity was unaffected by the load drop, remaining relatively constant to the end of the test. Group C also seemed unaffected by "drop 2" but was distinct as it had reduced activity after "drop 1" and increasing activity towards the end of the test especially after "drop 3".

AE groups show correlation to expected damage. A load drop indicates a sudden failure. Therefore, "drop 2" is expected to be the culmination of one damage type's evolution. AE has been shown to have a similar response, where the load drop was associated with the ending of group A. The load drop is also expected to be followed by redistribution of stresses, which can trigger the evolution of a different type of damage, alleviate the evolution of another, or have a small effect on another type of damage. AE has been shown to have similar three responses, where the load drop was associated with the initiation of group E, reduced activity of group B, and the unaffected continuation of group D.

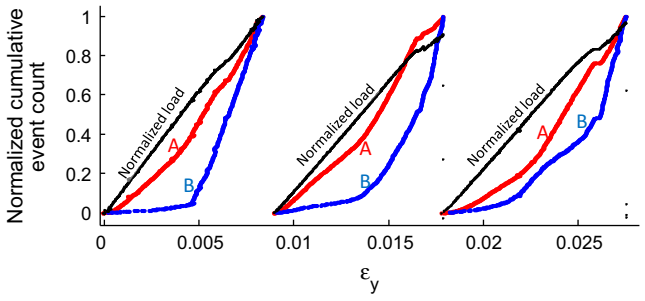

Fig. 13. Comparison of load response and AE analysis results for three identical experiments on samples with added plies.

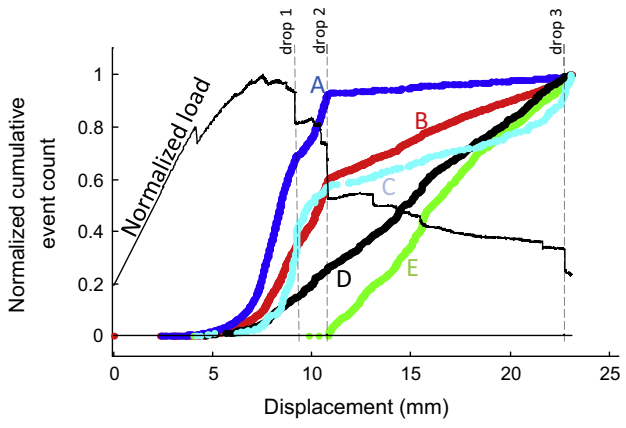

Fig. 14. AE activity history and load drops from 4-pt bending test.

5. Summary

This work presents an AE analysis approach that seeks to separate observations into the greatest number of clusters with distinct evolution behavior. Expectation–maximization is the technique used for the analysis with the assumption of Gaussian mixture distribution. Ten temporal and frequency domain AE features were used for describing observations. The proposed analysis was performed on AE acquired from tension and 4-point bending tests conducted on carbon fiber reinforce epoxy with the following configurations: unidirectional 0°, ±45°, and quasi-isotropic with ply-drop stress riser. The results show strong correlation between AE clusters and the mechanical response of the samples. The correlation indicates that AE events in different separated clusters are emitted from different damage mechanisms.

Acknowledgment

This work was supported by Honda R&D Americas Incorporated.

References

[1] Abry JC, Choi YK, Chateauminois A, Dalloz B, Giraud G, Salvia M. In-situ monitoring of damage in CFRP laminates by means of AC and DC measurements. Compos Sci Technol 2001;61(6):855–64.
[2] Ceysson O, Salvia M, Vincent L. Damage mechanisms characterisation of carbon fibre/epoxy composite laminates by both electrical resistance measurements and acoustic emission analysis. Scripta Mater 1996;34(8):1273–80.
[3] Schulte K, Baron C. Load and failure analyses of CFRP laminates by means of electrical resistivity measurements. Compos Sci Technol 1989;36(1):63–76.
[4] Guemes JA, Menéndez JM. Response of Bragg grating fiber-optic sensors when embedded in composite laminates. Compos Sci Technol 2002;62(7–8):959–66.
[5] Raju, Azmi Al, Prusty BG. Acoustic emission techniques for failure characterisation in composite top-hat stiffeners. J Reinforced Plast Compos 2012;31(7):495–516.
[6] Kim JH, Pierron F, Wisnom MR, Syed-Muhamad K. Identification of the local stiffness reduction of a damaged composite plate using the virtual fields method. Compos A 2007;38(9):2065–75.
[7] Arumugam V, Sajith S, Stanley AJ. Acoustic emission characterization of failure modes in GFRP laminates under Mode I delamination. J Nondestr Eval 2011;30(3):213–9.
[8] Sasikumar T, Rajendraboopathy S, Usha K, Vasudev E. Artificial neural network prediction of ultimate strength of unidirectional T-300/914 tensile specimens using acoustic emission response. J Nondestr Eval 2008;27(4):127–33.
[9] Prosser WH, Jackson KE, Kellas S, Smith BT. Advanced waveform-based acoustic emission detection of matrix cracking in composites. Mater Eval 1995;53(9):1052–8.
[10] Marec A, Thomas J-H, Guerjouma RE. Investigation of damage mechanisms of composite materials: multivariable analysis based on temporal and wavelet features extracted from acoustic emission signals. J Acoust Soc Am 2008;123(5):399–409.
[11] Kamala G, Hashemi J, Barhorst AA. Discrete-wavelet analysis of acoustic emissions during fatigue loading of carbon fiber reinforced composites. J Reinf Plast Compos 2001;20(3):222–38.
[12] Davijani AA, Bakhtiary, Hajikhani M, Ahmadi M. Acoustic emission based on sentry function to monitor the initiation of delamination in composite materials. Mater Des 2011;32(5):3059–65.
[13] Calabrese GCEPL. Noise removal by cluster analysis after long time AE corrosion monitoring of steel reinforcement in concrete. Constr Build Mater 2012;34(1):362–71.
[14] Maulik U, Bandyopadhyay S. Performance evaluation of some clustering algorithms and validity indices. IEEE Trans Pattern Anal Mach Intell 2002;24(12):1650–4.
[15] Duda RO, Hart PE, Stork DG. Pattern classification. 2nd ed. New York: Wiley; 2001.
[16] Sanchez-Hernandez G, Chiclana F, Agell N, Aguado JC. Ranking and selection of unsupervised learning marketing segmentation. Knowl-Based Syst 2013;44:20–33.
[17] Maul bT, Baba S. Unsupervised learning in second-order neural networks for motion analysis. Neurocomputing 2011;74(6):884–95.

[18] Mikheev A. Unsupervised learning of part-of-speech guessing rules. Nat Lang Eng 1996;2(2):111–36.
[19] MathWorks, K-means clustering – MATLAB kmeans, <http://www.mathworks.com/help/stats/kmeans.html> [accessed 21.03.2014].
[20] Farhidzadeh A, Dehghan-Niri E, Salamone S. Gaussian mixture modeling of acoustic emissions for structural health monitoring of reinforced concrete structures. Sens Smart Struct Technol Civ Mech Aerosp Syst 2013;8692.
[21] Pan B. Recent progress in digital image correlation. Exp Mech 2011;51(7):1223–35.
[22] Cardenas-Garcia JF, Yao HG, Zheng S. 3D reconstruction of objects using stereo imaging. Opt Lasers Eng 1995;22(3):193–213.
[23] Colombo S, Giannopoulos A, Forde MC, Hasson R, Mulholland J. Frequency response of different couplant materials for mounting transducers. NDT and E Int 2005;38(3):187–93.
[24] Bilmes JA. A gentle tutorial of the EM algorithm and its application to parameter estimation for gaussian mixture and hidden markov models. University of Berkeley; 1998.